CHEMISTRY OF MATERIALS
Article

Chem. Mater. **2010,** *22,* 1739–1748 1739
DOI:10.1021/cm9031557

Magnetic Resonance Imaging Contrast Agents Based on Iron Oxide Superparamagnetic Ferrofluids

Maria F. Casula,*[,†] Patrizia Floris,[†] Claudia Innocenti,[‡] Alessandro Lascialfari,[§,∥,⊥] Massimo Marinone,[§,∥] Maurizio Corti,[∥,⊥] Ralph A. Sperling,[⊗] Wolfgang J. Parak,[⊗] and Claudio Sangregorio[‡]

[†]*Dipartimento di Scienze Chimiche and INSTM, Università di Cagliari, Cittadella Universitaria, Monserrato, 09042 (CA), Italy,* [‡]*Dipartimento di Chimica and INSTM, Università di Firenze, Via della Lastruccia, 3, Sesto Fiorentino, 50019 (FI), Italy,* [§]*Dipartimento di Scienze Molecolari Applicate ai Biosistemi and INSTM, Università di Milano, Via Trentacoste 2, 20134 (MI), Italy,* [∥]*S3-CNR-INFM, Via Campi 213/A, 41125 (MI), Italy,* [⊥]*Dipartimento di Fisica "A. Volta" and INSTM, Università degli Studi di Pavia, Via Bassi 6, 27100 (PV), Italy, and* [⊗]*Philipps Universität Marburg, Renthof 7, 35032 Marburg, Germany*

Received October 13, 2009. Revised Manuscript Received December 16, 2009

Novel systems based on suspensions of colloidal magnetic nanoparticles have been investigated as perspective superparamagnetic contrast agents (CA) for magnetic resonance imaging (MRI). The nanostructures that we have studied contain surfactant-capped magnetite (Fe_3O_4) inorganic cores with different controlled sizes, ranging from 5.5 to 12 nm. The as-synthesized nanostructures are passivated by hydrophobic surfactants and thus are fully dispersible in nonpolar media. The magnetic nanocrystals have been transferred into aqueous media by a procedure based on the surface intercalation and coating with an amphiphilic polymer shell. The MRI efficiency in contrasting images, i.e., the NMR relaxivities r_1 and r_2, have been compared with Endorem and Sinerem, commercial superparamagnetic MRI contrast agents. We found that our nanostructures exhibit r_1 and r_2 relaxivities comparable to those of commercial CA over the whole frequency range. The MRI efficiency of our samples was related to their microstructural and magnetic properties. The transverse relaxivity r_2, leading the contrast in "negative" superparamagnetic agents, was found to improve as the diameter of the inorganic core is increased. The NMR relaxometry profile confirmed the nature of the physical mechanisms inducing the increase of the nuclear relaxation rates at low (magnetic anisotropy) and high (Curie relaxation) fields.

1. Introduction

Magnetic resonance imaging (MRI) is one of the most important medical noninvasive techniques for the diagnosis of many diseases in human soft tissues.[1] By this technique, information on healthy or diseased internal organs, cells, and tissues of the human body is easily obtained, with the highest resolution and the fastest collection times. The contrast of MRI images, based on the different distribution of hydrogen nuclei's spin density along the body, can be increased by using magnetic compounds, the so-called "contrast agents" (CAs),[2] that decrease the relaxation times of the nuclei present in the regions reached by CAs with respect to their natural value.[3,4] The contrast agents can be distinguished in "positive" (or T_1-relaxing), characterized by brilliant spots in the regions where they are delivered, and "negative" (or T_2-relaxing), which give dark zones where they accumulate. The positive CAs are based on paramagnetic compounds, whereas the negative ones are generally compounds with magnetic cores constituted by superparamagnetic (SP) ferrites. The negative CA can be further distinguished between superparamagnetic iron oxide particles (SPIO, average hydrodynamic radius $R_H > 15-20$ nm) and ultrasmall superparamagnetic iron oxide particles (USPIO, $R_H < 15$ nm). The available commercial compounds have the disadvantage of possessing a wide dispersion of particle size and a magnetic core constituted by more than one magnetic species (e.g., a mix of Fe_3O_4 and γ-Fe_2O_3), hampering therefore the possibility to relate their contrast efficiency to the fundamental chemico-physical properties. Current research on SP ferrite-based CAs is roughly following two main lines: synthesis of non-specific CAs, and synthesis of specific CAs. In the first case the main goal is to finely control the

*Corresponding author. E-mail: casulaf@unica.it.

(1) Rinck, P. A., Ed. *Magnetic Resonance in Medicine*, 3rd ed.; Blackwell: Oxford, U.K., 1993.
(2) Laurent, S.; Vander Elst, L.; Roch A.; Muller, R. N. In *NMR-MRI, μSR and Mossbauer Spectroscopies in Molecular Magnets*; Carretta, P., Lascialfari, A., Eds.; Springer-Verlag: Milano, Italy, 2007; p 71.
(3) Lascialfari, A.; Corti, M. In *NMR-MRI, μSR and Mossbauer Spectroscopies in Molecular Magnets*; Carretta, P., Lascialfari, A., Eds.; Springer-Verlag: Milano, Italy, 2007; p 89.
(4) Various authors in *The Chemistry of Contrast Agents in Medical Magnetic Resonance Imaging*; Merbach, A. E., Toth, E., Eds.; Wiley: New York, 2001.

Published on Web 01/19/2010

properties of the novel systems in order to increase the contrast in the MR images;[5−13] whereas in the latter case the target of specific cells, tissues, antigens, etc. (i.e. molecular imaging) is pursued, to evidence more clearly tumors, hemorrhages, local damages, etc.[14−17]

In this work, we address the understanding of the fundamental chemico-physical parameters acting on the nuclear relaxivity (i.e., the efficiency of the CAs), by synthesizing superparamagnetic iron oxide (SPIO) CAs, based on size-controlled colloidal nanocrystals (NCs). In particular, we have focused our attention on NCs with a nearly spherical morphology and a magnetite (Fe_3O_4) inorganic core with average diameters d = 5.5, 8.0, and 12.0 nm. The ability to control the size of the NCs, provided by the adopted synthetic technique, together with the control of the coating and the magnetic anisotropy should allow one to optimize the MRI contrast images by guiding the resulting nuclear relaxation. We chose iron oxides as magnetic cores because their medical use has been already approved by the U. S. Food and Drug Administration (FDA), envisaging a potential in vivo application for the material presented in this work. Moreover, the elucidation of the relaxometric behavior of magnetite provides grounds for the development of novel CAs based on magnetic substituted ferrites of the general formula MFe_2O_4, where M = Mn^{2+}, Zn^{2+}, or Co^{2+}.

Here we show the ability of the synthesized CAs in increasing the nuclear relaxation rates of the water protons, through the usual NMR-dispersion (NMRD) curves of the longitudinal (r_1) and transverse (r_2) relaxivities, defined as the increase of the relaxation rates per millimole of magnetic center. The NMRD results are compared with those obtained on standard SPIO and USPIO CAs, namely, Endorem and Sinerem (Guerbet Group, Roissy, France). A comparison among samples with different sizes suggests that all samples are efficient negative CAs, the best performance being obtained for d = 8−12 nm.

2. Experimental Section

Reference Materials. Endorem and Sinerem that were used as reference materials were purchased from the Guerbet Group (Roissy, France) and used without further purification.

Synthesis of Hydrophobic Iron Oxide Superparamagnetic Nanocrystals. The synthesis of iron oxide nanocrystals was carried according to a procedure previously reported[18] and gave rise to monodisperse hydrophobic iron oxide nanocrystals which produced stable colloidal suspensions in nonpolar solvents such as toluene. Briefly, sample preparation was carried out inside a drybox using airless procedures. In a typical synthesis, a solution of tridecanoic acid ($C_{13}H_{26}O_2$, 98%, Alfa Aesar) in octyl ether ($C_{16}H_{34}O$, 99%, Aldrich) is heated under Ar flow at 293 °C. A solution of iron pentacarbonyl ($Fe(CO)_5$, 99.5%, Alfa Aesar) in ether and a solution of the oxidizer (3-chloroperoxybenzoic acid, $C_7H_5O_2Cl$, 77% Aldrich) in ether were then rapidly coinjected. The overall iron molar concentration was 0.1 M, and the iron/surfactant/oxidizer molar ratios were 1:3:1.5. Under these conditions, a color change from yellow to dark is observed due to the formation of the nanocrystals. One minute after the solution turned dark, a further addition of oxidizer (0.5 of the moles of iron pentacarbonyl) was done to promote the formation of the desired iron oxide phase. After a suitable growth time at 293 °C, the solution was cooled down and the nanoparticles were precipitated from the solution and washed by addition of ethanol and centrifugation and redissolution in toluene. Because of the monodispersity of the nanoparticles, no further size selection procedure was needed.

The samples hereafter called SPION-1, SPION-2, and SPION-3, which differ in their mean particle size, were obtained after a growth time of 2, 5, and 8 min, respectively.

Synthesis of Hydrophilic Iron Oxide Superparamagnetic Nanocrystals. In order to transfer the nanoparticles into water, the surface modification of the SPION samples was performed in order to create an amphiphilic polymer shell which surrounds each nanocrystal.[19] A solution of poly(maleic anhydride alt-1-tetradecene) (Aldrich) in chloroform and a solution of iron oxide nanocrystals in chloroform (200 polymer units per square nanometer of effective nanocrystal surface) were mixed at room temperature. After evaporation of the solvent, bis(6-aminohexyl)-amine in chloroform was then added to cross-link the polymer shell that had formed around each nanocrystal; a ratio of added cross-linker molecules to polymer units of 1:10 was used. The solvent was evaporated again, and the solid was dissolved in a diluted alkaline solution (pH 8−9) to promote hydrolyzation of the anhydride functional groups. As a consequence, the polymer shell becomes amphiphilic and therefore the nanocrystals dissolved completely. After sonication for a few minutes, the solution was filtered to remove the excess unbound polymer and then two rounds of dilution and reconcentration through a

(5) Song, H.-T.; Choi, J.-s.; Huh, Y.-M.; Kim, S.; Jun, Y.-w.; Suh, J.-S.; Cheon, J. *J. Am. Chem. Soc*. **2005**, *127*, 9992.
(6) Jun, Y. W.; Huh, Y.-M.; Choi, J. S.; Lee, J. H.; Song, H.-T.; Kim, S.; Yoon, S.; Kim, K.-S.; Shin, J.-S.; Suh, J.-S.; Cheon, J. *J. Am. Chem. Soc*. **2005**, *127*, 5732.
(7) Taboada, E.; Rodriguez, E.; Roig, A.; Orò, J.; Roch, A.; Muller, R. N. *Langmuir* **2007**, *23*, 4583.
(8) Laurent, S.; Forge, D.; Port, M.; Roch, A.; Robic, C.; Vander Elst, L.; Muller, R. N. *Chem. Rev*. **2008**, *108*, 2064.
(9) Tromsdorf, U. I.; Bigall, N. C.; Kaul, M. G.; Bruns, O. T.; Nikolic, M. S.; Mollwitz, B.; Sperling, R. A.; Reimer, R.; Hohenberg, H.; Parak, W. J.; Forster, S.; Beisiegel, U.; Adam, G.; Weller, H. *Nano Lett*. **2007**, *7*, 2422.
(10) Berret, J.-F.; Schonbeck, N.; Gazeau, F.; El Kharrat, D.; Sandre, O.; Vacher, A.; Airiau, M. *J. Am. Chem. Soc*. **2006**, *128*, 1755.
(11) Corti, M.; Lascialfari, A.; Micotti, E.; Castellano, A.; Donativi, M.; Quarta, A.; Cozzoli, P. D.; Manna, L.; Pellegrino, T.; Sangregorio, C. *J. Magn. Magn. Mater*. **2008**, *320*, e320.
(12) Lartigue, L.; Oumzil, K.; Guari, Y.; Larionova, J.; Guérin, C.; Montero, J.-L.; Barragan-Montero, V.; Sangregorio, C.; Caneschi, A.; Innocenti, C.; Kalaivani, T.; Arosio, P.; Lascialfari, A. *Org. Lett*. **2009**, *11*, 2992.
(13) Figuerola, A.; Fiore, A.; Di Corato, R.; Falqui, A.; Giannini, C.; Micotti, E.; Lascialfari, A.; Corti, M.; Cingolani, R.; Pellegrino, T.; Cozzoli, P. D.; Manna, L. *J. Am. Chem. Soc*. **2008**, *130*, 1477.
(14) Caravan, P.; Das, B.; Dumas, S.; Epstein, F. H.; Helm, P. A.; Jacques, V.; Koerner, S.; Kolodziej, A.; Shen, L.; Sun, W.-C.; Zhang, Z. *Angew. Chem*. **2007**, *119*, 8319.
(15) Flacke, S.; Fischer, S.; Scott, M. J.; Fuhrhop, R. J.; Allen, J. S.; McLean, M.; Winter, P.; Sicard, G. A.; Gaffney, P. J.; Wickline, S. A.; Lanza, G. M. *Circulation* **2001**, *104*, 1280.
(16) Terreno, E.; Delli Castelli, D.; Cabella, C.; Dastru, W.; Sanino, A.; Stancanello, J.; Tei, L.; Aime, S. *Chem. Biodiversity* **2008**, *5*, 1901.
(17) Bruns, O. T.; Ittrich, H.; Peldschus, K.; Kaul, M. G.; Tromsdorf, U. I.; Lauterwasser, J.; Nikolic, M. S.; Mollwitz, B.; Merkell, M.; Bigall, N. C.; Sapra, S.; Reimer, R.; Hohenberg, H.; Weller, H.; Eychmuller, A.; Adam, G.; Beisiegel, U.; Heeren, J. *Nat. Nanotechnol*. **2009**, *4*, 192.
(18) Casula, M. F.; Jun, Y.-w.; Zaziski, D. J.; Chan, E. M.; Corrias, A.; Alivisatos, A. P. *J. Am. Chem. Soc*. **2006**, *128*, 1675.
(19) Pellegrino, T.; Manna, L.; Kudera, S.; Liedl, T.; Koktysh, D.; Rogach, A. L.; Keller, S.; Radler, J.; Natile, G.; Parak, W. J. *Nano Lett*. **2004**, *4*, 703.

centrifuge filter were performed. After such purification, the nanocrystals solutions were optically clear. Samples after water transfer will be called W-SPION.

Sample Characterization. Transmission electron microscopy (TEM) micrographs in the bright field (bf) mode together with selected area electron diffraction (saed) were recorded on a JEOL 200CX microscope operating at 200 kV. A drop of the toluene- or water-based suspension of the iron oxide nanocrystals was deposited and dried at room temperature on a carbon-coated copper grid.

X-ray powder diffraction (XRD) patterns were recorded using Cu Kα radiation on a X3000 Seifert diffractometer equipped with a graphite monochromator on the diffracted beam. The nanocrystals were deposited on a zero-background sample holder after precipitation. Phase identification was performed according to the Powder Diffraction File database.[20]

Dynamic light scattering (DLS) and ζ potential measurements were performed with a Zetasizer Nano ZS (Malvern Instruments) provided with a laser of 633 nm wavelength. The measurements on the initial colloidal dispersions of hydrophobic nanocrystals dispersed in toluene was performed using a glass cuvette, whereas the water dispersions of the polymer-coated nanocrystals were characterized in a disposable "Size & Zeta" folded capillary cell cuvette equipped for simultaneous Z-potential determination. The intensity averaged diameter values were taken into account.

Inductively coupled plasma-optic emission spectrometry (ICP-OES, Perkin-Elmer Optima 2000) was used to analyze the suspension of the nanoparticles prior and after water transfer. The Fe analysis provided the value of the metal concentration in solution for the relaxometric studies.

Measurements of static magnetizations and hysteretic behavior were performed by a Cryogenic S600 SQUID magnetometer equipped with a superconducting magnet producing fields up to 6.5 T. Zero-field-cooled (ZFC) magnetizations were measured by cooling samples in zero magnetic field and then by increasing the temperature in the presence of a 5 mT field, whereas field-cooled (FC) curves were recorded by cooling the samples in the same probe field of 5 mT. The field dependence of the magnetization (hysteresis loop) was recorded up to ±6.5 T, at $T = 3.0$ K. All data were corrected for the diamagnetism of the solvents and of the sample holder which were separately determined in the same temperature and field ranges. Alternating current (ac) susceptibility measurements were performed using a homemade probe inserted in an Oxford cryostat working in the 50−25 000 Hz.[21]

The ^{1}H nuclear magnetic resonance (NMR) relaxometry characterization (NMR-dispersion profile) was performed at physiological and room temperature by measuring the longitudinal and the transverse nuclear relaxation times T_1 and T_2 in the frequency range 10 kHz ≤ ν ≤ 65 MHz for T_1 and 10 MHz ≤ ν ≤ 60 MHz for T_2. The range of frequency has been chosen on the basis of two different reasons: (a) to cover the frequencies corresponding to the most used clinical fields, i.e., 0.2 (∼8 MHz), 0.5 (∼20 MHz), and 1.5 T (∼64 MHz) and (b) to have data for studying the mechanims that lead to the nuclear relaxation, through the analysis of the behavior of $r_1(\nu)$ and $r_2(\nu)$ curves (see below). It should be noticed that the measurements at room and physiological temperatures gave the same results within 10%. The NMR signal detection and generation was obtained by a Smartracer Stelar relaxometer (which makes use of the fast-field-cycling technique) for 10 kHz ≤ ν ≤ 10 MHz,[22] a Stelar Spinmaster and an Apollo-Tecmag Fourier transform-nuclear magnetic resonance (FT-NMR) spectrometer for $\nu > 10$ MHz. In the second case, standard radio frequency excitation sequences Carr-Purcell-Meiboom-Gill (CPMG)-like (T_2) and of saturation-recovery (T_1) were used.

To determine the efficiency of MRI contrast agents, we have calculated the nuclear relaxivities, both longitudinal, r_1, and transverse, r_2, defined as

$$r_i = [(1/T_i)_{meas} - (1/T_i)_{dia}]/c \quad i = 1, 2$$

where $(1/T_i)_{meas}$ is the value measured for the sample with concentration c (mmol L^{-1}) of magnetic center (see Table 1), and $(1/T_i)_{dia}$ represents the nuclear relaxation rate of the diamagnetic host solution (water or toluene in our case). The concentration c of Fe ions is 2−3 orders of magnitude larger that the concentration of iron oxide nanocrystals and is reported in Table 1 for all the investigated samples.

Table 1. Concentration of Iron in the Investigated Samples, Dispersed Either in Toulene or in Water

sample	dispersant	concentration of Fe (mg/L)
(d = 5.5 nm) SPION 1	toluene	926.9
(d = 5.5 nm) W-SPION 1	water	64.8
(d = 8.0 nm) SPION 2	toluene	1066.0
(d = 8.0 nm) W-SPION 2	water	144.13
(d = 12.0 nm) SPION 3	toluene	613.7
(d = 12.0 nm) W-SPION 3	water	190.0
Endorem	water	11 200 (given by the supplier)
Sinerem	water	20 000 (given by the supplier)

The MRI images of a phantom containing four vials with our three samples in water (W-SPION1, W-SPION2, and W-SPION3, see later on) and the commercial compound Endorem have been collected with an Artoscan 0.2 T Imager by Esaote. The sequence used was a Gradient-Echo T_2*-weighted sequence with TE = 16 ms, TR = 1 s. For the sake of direct comparison, all four samples have been diluted to the same concentration $c \sim 0.020$ mg/mL.

Results and Discussion

Characterization and Relaxometric Properties of Hydrophobic Colloidal Nanocrystals. Figure 1 shows representative bright field TEM images of the SPION samples, indicating that the nanocrystals are faceted and nearly monodisperse in size. The particle size increases from sample SPION-1 to sample SPION-3, the average diameter going from 5.5 to 8.0 nm to 12.0 nm, according to the size distribution obtained by statistical analysis of the images.

The XRD patterns of the samples, reported in Figure 2, are very similar and show broad reflections due to the presence of a nanocrystalline iron oxide spinel phase. The observed pattern can be ascribed either to the γ polymorph of the ferric oxide (γ-Fe_2O_3, maghemite) or the mixed valence iron oxide (Fe_3O_4, magnetite) as these phases cannot be discriminated by X-ray powder diffraction in nanocrystalline samples due to the extra line broadening of the peaks. Spectroscopic characterization techniques such as Raman, Mossbauer, and X-ray

(20) PDF-2 File. ICDD International Centre for Diffraction Data, 1601 Park Lane, Swarthmore, PA.
(21) Midollini, S.; Orlandini, A.; Rosa, P.; Sorace, L. *Inorg. Chem.* **2005**, *44*, 2060.
(22) Ferrante, G.; Sykora, S. *Adv. Inorg. Chem.* **2005**, *57*, 405.

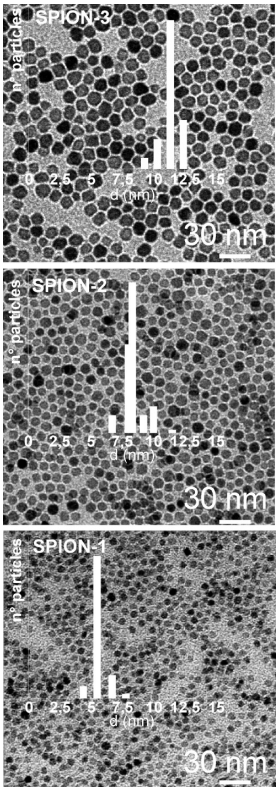

Figure 1. Transmission electron microscopy bf images of SPION-1, SPION-2, and SPION-3 (from bottom to top) and corresponding particle size distribution (insets) obtained by statistical analysis over ~150 particles.

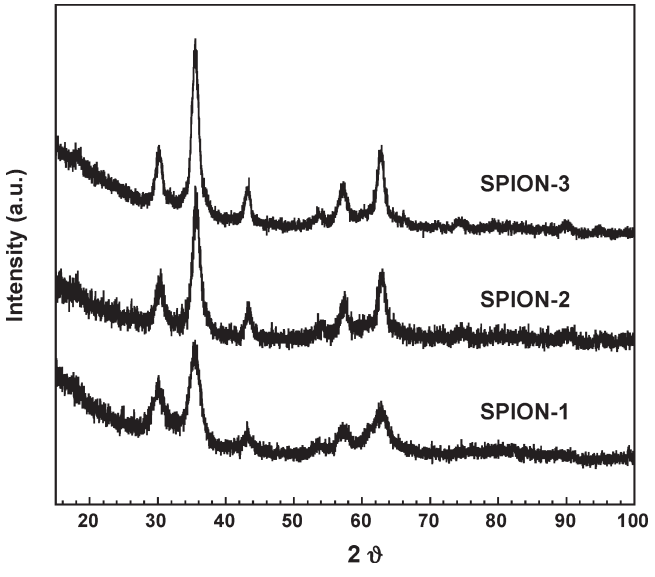

Figure 2. X-ray diffraction patterns of samples SPION-1, SPION-2, and SPION-3 (from bottom to top) obtained using Cu Kα radiation.

absorption (XAFS) can be effectively used to identify the iron oxide spinel structure. Raman and XAFS spectroscopy measurements on other samples prepared by the same synthetic protocol suggests that the magnetite Fe_3O_4 phase is mainly present.[18,23] The peak broadening decreases from SPION-1 to SPION-3, indicating a progressive increase in the average particle size, in agreement with TEM observations. The average particle size as determined by the Scherrer equation from line broadening of the 311 reflection ($2\theta \sim 35.5$) was of 5.5, 8.0, 10.0 nm for sample SPION-1, SPION-2 and SPION-3, respectively.

The samples gave stable colloidal dispersions in nonpolar solvents such as toluene and chloroform thanks to the hydrophobic capping agent present on the surface. The toluene suspensions were characterized by DLS in order to gain insights on the dynamic diameter of the SPION samples. All the samples have a relatively narrow and symmetrical distribution which is centered at 8.6, 12.0, and 14.9 nm for SPION-1, SPION-2, and SPION-3. These data are in agreement with the other structural data, taking into account that the tridecanoic acid used as a capping agent on the surface of the nanocrystals has a length of about 1 nm.

The magnetic properties of the samples were investigated by measuring the ZFC-FC magnetization curves. The collected data for the colloidal suspension of the three SPION samples are reported in Figure 3A. The two curves superimpose at temperatures above the so-called separation temperature, T_{SEP}. The ZFC curve exhibits a maximum at the temperature $T_B < T_{SEP}$, and these two temperatures together with the shape of the magnetization curves provide insights on the superparamagnetic behavior of the samples. The observed behavior is representative of superparamagnetic materials and accordingly T_B increases with the NCs size. For all the samples, T_B is well below room temperature, indicating that the synthesized SPION samples are in the superparamagnetic state at physiological temperature, as required for in vivo applications. Moreover, thermal irreversibility develops at temperatures close to T_B indicating a narrow distribution in the blocking energy of the NCs which can in turn be ascribed to the high crystallinity and narrow size distribution of the samples.

The M vs H curves collected at room temperature confirm that all the samples are in the superparamagnetic deblocked state (no coercivity). On the other hand, the hysteresis loops are open at 3 K (Figure 3B) with coercive fields, $\mu_0 H_c$, in the 33−45.5 mT range, increasing with the particle size. The colloidal suspensions are quite dilute, and therefore the occurrence of strong dipolar interactions can be ruled out (see also the Supporting Information). The same trend described for the colloidal suspensions was observed for the dried powders of the three SPION samples (see Figure S1, Supporting Information). However, in this case, significant dipolar interactions among the nanocrystals are observed. As a result, the blocking temperatures are higher and the coercive fields lower in the powder samples. Alternating current susceptibility measurements were performed on powder samples. The analysis of the data of SPION-1 (Figure S2 in the Supporting Information) provided a magnetic anisotropy energy density, K, of 9.3×10^4 J/m^3 and a pre-exponential attempt time for the magnetic moment

(23) Corrias, A.; Mountjoy, G.; Loche, D.; Puntes, V.; Falqui, A.; Zanella, M.; Parak, W. J.; Casula, M. F. *J. Phys. Chem. C* **2009**, *113*, 18667.

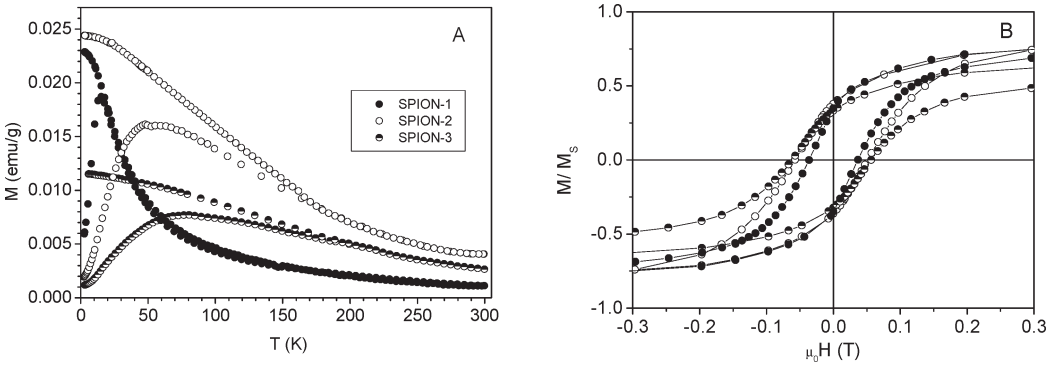

Figure 3. Zero field cooled and field cooled magnetization curves (A) and hysteresis curves at 3 K (B) for the SPION samples. The magnetization values in panel B are normalized to the corresponding saturation values which were extrapolated from the data for $1/H \rightarrow 0$ (however, all the curves are very close to saturation at the highest measuring field of 6.5 T). For the purpose of clarity, only the enlargement of the loops between ±0.3 T is shown, whereas the full loops are shown in the Supporting Information.

Table 2. Average NC Size As Determined by TEM and XRD, Average Hydrodynamic Diameter Obtained by DLS and Corresponding Magnetic Properties of the SPION Samples Obtained from the ZFC-FC Magnetization Curves and Hysteresis Loops Collected at 3 K

sample name	$\langle d \rangle_{TEM}$ (nm)	$\langle d \rangle_{XRD}$ (nm)	$\langle d \rangle_{DLS}$ (nm)	T_B (K)	$\mu_0 H_c$ (mT)	Mr/Ms
SPION-1	5.5	5.5	9	15	36.5	0.35
SPION-2	8.0	8.0	12	50	55.5	0.38
SPION-3	12.0	10.0	15	78	59.5	0.33

reversal, τ_0 of the order of 10^{-14} s. The K value is larger than the bulk one, as usually observed for magnetic NPs where the large surface contribution enhances the total effective anisotropy. However, the τ_0 value is smaller than those commonly observed for not-interacting single domain nanoparticles (10^{-9}–10^{-11} s) indicating that the relaxation dynamics is perturbed by interparticle interactions.[24] This suggest that the increase of the K value can be partial due to interactions. On the contrary, the same analysis on the other two powdered samples gave unphysical values for both parameters suggesting that, due to the larger magnetic moment, the reversal process is governed by very strong dipolar interactions among the nanoparticles, in good agreement with the T_{max} trend observed from ZFC measurements. Table 2 reports a summary of the main structural features and of the corresponding magnetic parameters for the SPION samples.

The longitudinal r_1 and transverse r_2 relaxivities of samples in toluene suspension are reported in Figure 4, for samples with different diameters and for the CAs used as a reference. Although a direct comparison between the suspensions in toluene and the commercial water-based suspensions is improper, insights on the mechanisms of relaxation in the different samples can be obtained. In particular, the observed frequency behavior of r_1 is very similar to that measured for water dispersion of commercial CAs Endorem and Sinerem. As the $r_1(\nu)$ behavior reveals the physical mechanisms that induce the relaxation of the nuclear magnetization, we can infer that in our samples these mechanisms are the same hypothesized for commercial CAs. In particular, the Curie relaxation

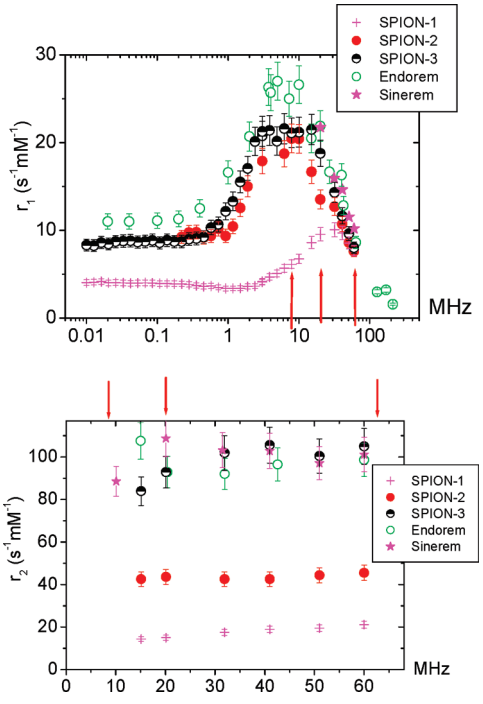

Figure 4. Longitudinal r_1 (upper) and transverse r_2 (bottom) relaxivities in iron oxide samples with different diameters, dispersed in toluene; the data are compared with the ones measured for two commercial compounds. The arrows indicate the most commonly used clinical fields.

dominates for frequencies $\nu > 5$–20 MHz, while for lower frequencies the nuclear relaxation is due to the Néel reversal of the particle magnetization, determined by the magnetic anisotropy.[8,25] The most important parameter for negative CAs, however, is the increase of T_2-relaxation per millimole of magnetic center, i.e., r_2. Thus the results of Figure 4 suggest that in the frequency range of clinical use (indicated by the arrows in the figure) the most promising CAs are SPION-2 (d = 8 nm) and SPION-3 (d = 12 nm) whose r_2 values are not far from the ones of Endorem and Sinerem.

In Table 3, the r_2/r_1 ratio for the different samples is given; as it can be easily seen, the values obtained are all greater than 2, i.e., roughly the threshold value for effective negative contrast. The ratio r_2/r_1 is thus an efficiency parameter providing a precise idea of how

(24) Dormann, J. L., Fiorani, D., Tronc, E. *Adv. Chem. Phys.*, Vol. *XCVIII*; Prigogine, I., Rice, A., Eds.; Wiley: New York, 1997.

(25) Roch, A.; Muller, R. N.; Gillis, P. *J. Chem. Phys.* **1999**, *110*, 5403.

Table 3. Ratio between Longitudinal and Transverse Relaxivity of the SPION Samples at Given Fields $H \sim 0.47$ T (20 MHz) and $H \sim 1.4$ T (60 MHz)

sample name	$(r_2/r_1)_{20\ MHz}$	$(r_2/r_1)_{60\ MHz}$
SPION-1	1.57	2.75
SPION-2	3.23	5.99
SPION-3	4.95	13.08

much nuclear longitudinal magnetization is available after each subsequent acquisition for averaging the signal. In our case such ratio increases with the average volume, V, of the NPs. As the magnetic anisotropy energy barrier, Δ, depends on the volume, through the relation $\Delta = KV$, this result points out the dominant role of the magnetic moment of the single particles in leading r_2/r_1.

From the above discussion it can be concluded that the SPION samples dispersed in toluene own the required features in terms of crystal structure, size and shape control, and magnetic properties to be considered as promising negative CA for magnetic resonance imaging. Moreover, the significant relaxivity difference observed among the investigated samples provides insights on the mechanisms determining the relaxometric efficiency. Therefore, in view of perspective biomedical applications and in order to effectively compare our materials with commercially available CAs, we have transferred our materials in water medium.

Characterization and Relaxometric Properties of Hydrophilic Colloidal Nanocrystals. The preparation of water-based suspension of the iron oxide NCs (W-SPION) was performed by means of an amphiphilic polymer (poly(maleic anhydride)) which wraps the whole original hydrophobic NC by intercalation of the hydrophobic alkyl chains of the polymer into the hydrophobic coating of the iron oxide NCs. We chose to perform the phase transfer of the iron oxide NCs by this polymer coating procedure as it has proven to lead to colloids with high stability,[19] a key requirement in view of biomedical applications. One of the factors which contributes to the stability of the water based colloids obtained by this approach is that unlike other ligand exchange procedures, in this case the polymer coating occurs on top of the capped NC without replacing the original hydrophobic capping agent, preventing therefore agglomeration and precipitation processes. An additional advantage of this phase transfer procedure is that the polymer-coated NCs exhibit anhydride rings in the outer shell, which in aqueous media turn into carboxyl groups and can be further functionalized or coupled to biomolecules.[26] The polymer coating procedure leads to clear and stable water-based suspensions for all samples (shown in the Supporting Information, Figure S3). Characterization by TEM and XRD indicates that structural and morphological features of the samples are unaltered upon phase transfer. Representative TEM images of the W-SPION samples are reported in Figure 5 showing that no evidence of NC aggregates is observed. Agglomeration in solution was

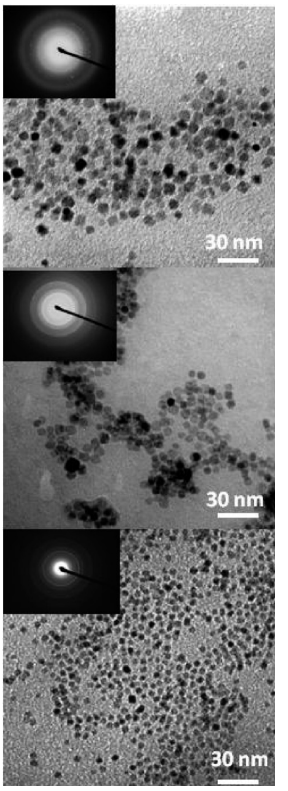

Figure 5. Transmission electron microscopy bright field images of samples W-SPION1, W-SPION2, and W-SPION3 (from bottom to top) and corresponding selected area electron diffraction (insets).

excluded by performing gel electrophoresis and size exclusion chromatography control experiments.[27] Single NC-polymer nanostructures could be obtained by using a dilute initial solution and by adopting the appropriate polymer/nanocrystals ratio, as described in the Experimental Section. As a consequence, the obtained water-based ferrofluids are significantly more dilute than the corresponding toluene suspensions. The electron diffraction patterns reported in the insets also show that the spinel structure is preserved. These results are in agreement with the data reported for NCs prepared by other routes and phase transferred by this approach, which indicate that the structural and morphological features of the original NCs are not affected by the polymer coating procedure.[9,11,19]

DLS measurements were performed in order to determine the hydrodynamic diameter of the W-SPION samples, obtaining a value of 32, 44, and 36 nm for the W-SPION1, W-SPION2, and W-SPION3 samples, respectively. The list of the hydrodynamic diameters together with the corresponding polydispersity index is reported in Table SI-1 in the Supporting Information together with the values obtained for the original toluene-base suspensions. However, we want to point out that absolute size measurements in the nanometer range with nanometer precision are generally complicated and thus have to be interpreted with care.[27] As expected, the

(26) Lin, C.-A. J.; Sperling, R. A.; Li, J. K.; Yang, T.-Y.; Li, P.-Y.; Zanella, M.; Chang, W. H.; Parak, W. J. *Small* **2008**, *4*, 334.

(27) Sperling, R. A.; Liedl, T.; Duhr, S.; Kudera, S.; Zanella, M.; Lin, C.-A. J.; Chang, W.; Braun, D.; Parak, W. J. *J. Phys. Chem. C* **2007**, *111*, 11552.

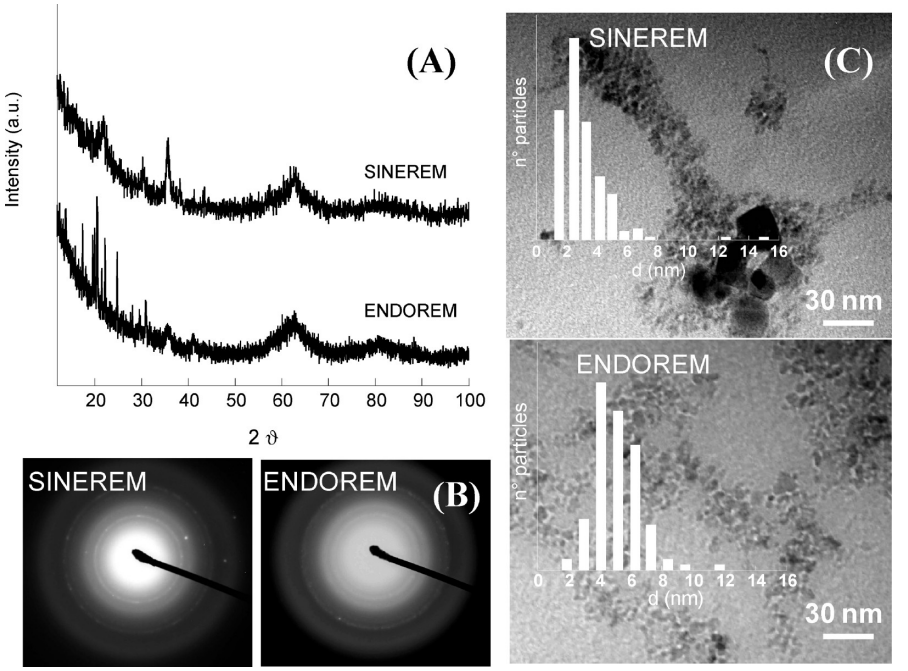

Figure 6. X-ray (A) and selected area electron (B) diffraction patterns, representative transmission electron microscopy images, and corresponding size distribution (C) for commercial Sinerem and Endorem.

hydrodynamic radius increases significantly with respect to the original SPION sample upon polymer coating. Previous studies have shown that the whole organic layer including the polymer shell around the inorganic nanocrystals has a thickness of roughly 4 nm. The increase found in this study is larger than expected on the basis of the size of the polymer; this has been previously observed and attributed to the change in particle−solvent interaction or to the contribution of small aggregates such as dimers,[19] whereas bigger aggregates can be strictly excluded from size exclusion chromatography experiments. It should be pointed out that for the W-SPION2 sample extra filtration by syringe filters was required, whereas the hydrodynamic diameter just after ultracentrifugation was ∼130 nm and did not vary upon dilution, suggesting that more nanoparticles were inglobated in the polymer coating. This can be due to the fact that the here used polymer coating had been optimized for nanocrystals with different organic capping. As for generality, the polymer-to-particle ratio also was not adjusted for nanocrystals of different size and the scenario of having sometimes several nanoparticles in one polymer shell is likely. However, it should be pointed out that DLS easily overestimates the contribution of agglomerates. A ζ potential of about −40 mV was found for all the W-SPION dispersions. These data indicating negative surface charge are in agreement with the stability of the colloidal suspension,[7] which in this case is mainly related to the charge repulsion among the deprotonated carboxylic groups on the NC surface.

In order to carry out a significant comparison between the W-SPION samples and the commercially available CA used as a reference, the structural characterization of Endorem and Sinerem by XRD, TEM, and DLS measurements was also performed prior to their magnetic and relaxometric characterization. Figure 6A shows the XRD patterns of Endorem and Sinerem: the sharp peaks present at low θ are due to the presence of the organics used as nanoparticle coating since the commercial samples were deposited as purchased, without further purification. The XRD patterns of Endorem and Sinerem are quite similar and show the presence of very broad peaks which are consistent with the presence of a spinel phase with nanocrystalline domains of similar size. Accurate determination of the nanocrystalline domain size by XRD data was not possible due to the small crystal size together with poor crystallinity of the samples. Selected area electron diffraction (shown in Figure 6B) also confirms the presence of the reflections of the spinel nanophase. Figure 6C reports typical bright field TEM observations of Sinerem and Endorem, which show in both samples the presence of nanoparticles with a not very well-defined morphology and no evident aspect ratio. The average particle size is slightly larger for the Endorem than for the Sinerem sample, as determined by analysis of the particle size distribution (7.5 vs 4.5 nm). As shown in Figure 6C, the particle size distribution for both reference samples is much broader than those of the synthesized SPION samples. The hydrodynamic diameter as determined by DLS were found to be 34 and 292 nm for Sinerem and Endorem, respectively; therefore, as expected Sinerem lies in the USPION and Endorem in the SPION colloids classes, respectively.

The structural and morphological results are in agreement with previously reported data,[28,29] which report that Endorem and Sinerem are dextran-coated nonstoichiometric magnetite crystalline cores of roughly 5−6 nm with

(28) Jung, C. W.; Jacobs, P. *Magn. Reson. Imaging* **1995**, *13*, 675.
(29) Jung, C. W. *Magn. Reson. Imaging* **1995**, *13*, 675.

Table 4. Average NC Size as Determined by TEM, Average Hydrodynamic Diameter Obtained by DLS, and Corresponding Magnetic Properties of the Commercial Samples Obtained from the ZFC-FC Magnetization Curves and Hysteresis Loops Collected at 3 K

sample name	$\langle d \rangle_{TEM}$ (nm)	$\langle d \rangle_{DLS}$ (nm)	ζ potential (mV)	T_B (K)	$\mu_0 H_c$ (mT)	Mr/Ms	KV/k_B	$\tau_0(10^{-11}$ s)
Sinerem	4.5	34	-12.6 ± 1.8	73	19.3	0.38	1775	0.32
Endorem	5.7	292	-15.6 ± 1.7	39	32.0	0.35	725	1.0

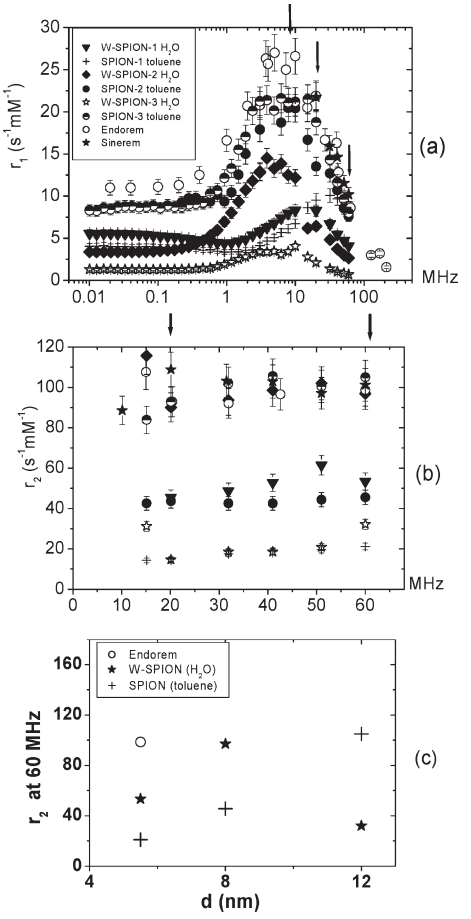

Figure 7. (a) Longitudinal, r_1, and (b) transverse, r_2, relaxivities for iron oxide samples dispersed in water, compared to the same samples in toluene and to commercial CA. (c) r_2 behavior as a function of the mean diameter *d*. The arrows indicate the frequencies of the most commonly used MRI clinical imagers.

no direct covalent bonding between the inorganic core and the dextran coating. Sinerem is found to be made out of single nanoparticles surrounded by a relatively thick layer of dextran, whereas in Endorem aggregates are coated by a thinner dextran layer, and a hydrodynamic diameter of 228 and 50 nm was found for Endorem and Sinerem, respectively.[28,29]

The magnetic features of these contrast agents were investigated by means of ZFC-FC magnetization and hysteresis measurements (see Figure S4 in the Supporting Information). Our data collected on Endorem resulted strictly similar to the ones reported in the literature.[30] The most relevant parameters for Sinerem and Endorem, as obtained from both static (ZFC/FC and hysteresis loop) and dynamic (ac susceptibility) magnetic measurements, are summarized in Table 4 together with the structural and morphological data.

(30) Gamarra, L. F.; Brito, G. E. S.; Pontuschka, W. M.; Amaro, E.; Parma, A. H. C.; Goya, G. F. *J. Magn. Magn. Mater.* **2005**, *289*, 439.

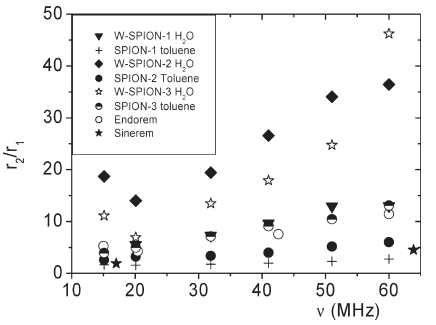

Figure 8. Ratio r_2/r_1 of iron oxide nanocrystals in aqueous suspensions, for different diameters of the magnetic core, in the investigated frequency range.

The magnetic characterization was performed on the water dispersions of the polymer coated SPION samples. These measurements indicate that the magnetic properties of all the samples are preserved as no noticeable differences emerge with respect to the corresponding toluene suspensions (see Supporting Information, Figure S5).The only exception is given by the ZFC-FC magnetization curves of W-SPION2 where the ZFC maximum is ~40 K larger than the original SPION-2 sample (from 50 K to 90 K). In our opinion, such an increase can be ascribed to the effect of strong interparticle interactions arising from the presence of large aggregates, as suggested by DLS measurements and by the effect of strong dipolar interactions on the magnetic properties of the powder SPION-2 sample, where the ZFC maximum temperature is as large as 127 K. On the other hand, the similarity observed for the other two samples confirms that no dipolar interactions are operating when the particle are dispersed in solution, both in toluene and in water.

The samples dispersed in water have been characterized by NMR relaxometry: the relaxivities are reported in Figure 7. In this Figure, the three different samples W-SPION1, W-SPION2, and W-SPION3 dispersed in water are compared to the same original samples in toluene and to the commercial CAs. The obtained results indicate that the polymer coating-guided phase transfer procedure does not alter the frequency dependence of $r_{1,2}$ for all samples. On the other hand, the absolute values of $r_{1,2}$ are different for the water colloidal with respect to the original toluene suspensions, likely due to the effect of possible agglomeration of more than one magnetic nanoparticle within the polymer coating and to the variation of the distance between the magnetic center and the relaxing nuclei. Interestingly, the sample W-SPION2 (dispersed in water) has r_2 values comparable to commercial compounds in the whole frequency range. Figure 8 points out that all the samples have a good r_2/r_1 ratio, and its frequency dependence confirms that the samples retain typical values of superparamagnetic CA after being

Figure 9. MRI images on three different samples plus Endorem, at the same concentration of Fe. The sequence used was a gradient-echo and the experimental parameters were TE = 16 ms, TR = 1000 ms. The upper sample is Endorem while in the lower raw, from left to right, the samples are W-SPION1, W-SPION2, and W-SPION3.

transferred into water phase. The values of r_2/r_1 are higher than or comparable to the ones of samples in the nonpolar phase and the ones of commercial CAs. This is particularly remarkable for sample with d = 12 nm W-SPION3 (which at high fields reaches the highest value) and for W-SPION2, in the whole frequency range.

Finally, it is interesting to analyze the r_2 behavior as a function of the particle size, d (Figure 7c). In the case of samples in toluene, r_2 increases monotonically with d reaching the maximum at d = 12 nm, while in the water-dispersed samples r_2 has a maximum at d = 8 nm, i.e., a nonmonotonic behavior. This discrepancy is difficult to be fully justified and requires further investigation. Nevertheless a qualitative interpretation can be attempted considering that different regimes are predicted for r_2 depending on the particle size.[31] For small particles dispersed homogeneously in solution, the systems are in the so-called "motional averaging regime" (MAR), where water diffusion between particles occurs on a much faster time scale than the resonance frequency shift. In this regime, the transverse relaxivity r_2 increases with increasing the particle size. For larger particles, the relaxation rate r_2 is given by the "static dephasing regime" (SDR) (introduced by Yablonskiy and Haacke),[32] where the large magnetic moment of the particles produces strong dipolar fields in its surroundings so that diffusion has a small influence on the decay of the nuclear magnetic resonance (i.e., on T_2, thus on r_2). In the SDR, r_2 reaches a plateau.[9,31,32] In our case, we observe a monotonic increase for samples in toluene, i.e., a MAR regime, while the maximum in $r_2(\nu)$ in water dispersed samples seems to indicate a change of regime at $d \sim 8$ nm. The theory explaining this situation is still under evaluation.

To validate our findings on the (r_2) efficiency of our samples in contrasting MRI images, we have collected MRI images at 0.2 T on an Artoscan Imager, commonly used for clinical investigation of diseases in articulations. As described in the Experimental Section, four vials, each one containing a different sample at the same Fe concentration, namely, Endorem, W-SPION1, W-SPION2, and W-SPION3 (see Figure 9) were put in the center of the detection coil. It can be easily seen that the sample W-SPION2 gives T_2*-weighted images as dark as (if not slightly darker than) the ones given by Endorem. These results confirm the efficiency of the prepared ferrofluid in enhancing the negative contrast in magnetic resonance images.

Conclusions

Stable suspensions of magnetic nanocrystalline ferrites have been synthesized and investigated as potential contrast agents for magnetic resonance imaging. We have prepared iron oxide magnetic NCs by rapid decomposition of iron pentacarbonyl into a hot solvent containing an oxidizer and a coordinating surfactant. By this procedure we have obtained nearly monodisperse capped NPs with three different size and well-defined crystallinity. In view of in vivo application, a polymer-coating surface modification procedure was performed which gave rise to stable suspensions in water phase. The NCs are superparamagnetic at room temperature, as required for biomedical use, and the corresponding efficiency as CA was studied by measuring the nuclear longitudinal and transverse relaxivities. All samples showed a relaxivities ratio $r_2/r_1 > 2$, putting them in the category of negative contrast agents, this ratio increasing with the inorganic core diameter. The highest r_2 value has been obtained for W-SPION2 sample (in water) with average diameter of the inorganic core $d \sim 8$ nm. In addition W-SPION2 and W-SPION3 samples also exhibit the

(31) Gillis, P.; Moiny, F.; Brooks, R. A. *Magn. Reson. Med.* **2002**, *47*, 257.
(32) Yablonskiy, D. A.; Haacke, E. M. *Magn. Reson. Med.* **1994**, *32*, 749.

largest r_2/r_1 ratio, which is an efficiency parameter for negative contrast.

MRI images collected in vitro at 0.2 T on phantoms containing the water-based ferrofluid samples and Endorem (as a reference), confirmed that W-SPION2 sample has a very good contrasting efficiency. Thus, we can conclude that the NCs with diameter of the inorganic core in the range 8−12 nm are very effective in increasing the nuclear relaxivities, being at the top-edge of the most efficient MRI contrast agents.

The structural, magnetic, and relaxometric study of the currently synthesized systems is a step toward a comprehensive and quantitative understanding of the dependence of the relaxivities on the magnetic and chemico-physical characteristics (size of the magnetic core, kind of magnetic ion, kind of coating, hydrodynamic radius, etc.) of magnetic NCs. Moreover, the relatively high anisotropy of these NCs make them interesting candidates as possible bifunctional systems, where the (MRI) diagnostic ability is associated to the possibility of using the ferrite as an agent for magnetic fluid hyperthermia.

Acknowledgment. This work was supported by the Università di Cagliari (Fondi 5%) and by INSTM-Consorzio Interuniversitario per la Scienza e Tecnologia dei Materiali, under the PRISMA project. Professors S. Aime and G. Poletti are gratefully acknowledged for helpful discussions. Thanks are due to T. Kalaivani, P. Arosio, and F. Orsini for support in experimental measurements. H. Amiri is gratefully acknowledged for help in MRI measurements on phantoms. Additional funds were provided by the Network of Excellence MagmaNet (Grant NMP3-CT-2005 515767).

Supporting Information Available: Magnetic characterization of the powder iron oxide samples and hysteresis loops for the toluene colloidal suspensions, image of the transfer into water media of the iron oxide nanocrystals and DLS characterization of the nonpolar and aqueous suspensions, ZFC-FC magnetization curves for the W-SPION samples and for the water-based commercial contrast agents (PDF). This material is available free of charge via the Internet at http://pubs.acs.org.